Radio-Channel Characterization of an Underground Mine at 2.4 GHz

Chahé Nerguizian, *Member, IEEE*, Charles L. Despins, *Senior Member, IEEE*, Sofiène Affès, and Mourad Djadel

***Abstract*—This paper presents comprehensive experimental results obtained from narrowband and wideband radio-channel measurements in an underground mine with narrow veins at 2.4 GHz. From continuous-wave (CW) measurement data, large-scale distance–power curves and path-loss exponents of the environment are determined. Other relevant parameters, such as the mean excess delay, the maximum excess delay, the root-mean-square (rms) delay spread, and the coherence bandwidth are extracted from the wideband-measurement data. Results show a propagation behavior that is specific for these underground environments with rough surfaces. The rms delay spread does not follow a dual-slope relation with respect to distance, as in environments with smooth surfaces. Moreover, the dependence of the rms delay spread on the bidimensional position of the user is found to be very significant. For the majority of locations, the rms delay-spread values are less than 60 ns.**

***Index Terms*—Channel path loss, multipath time dispersion, radio propagation parameters, ultrahigh frequency (UHF) narrowband and wideband measurements, underground mine.**

I. Introduction

TRULY ubiquitous wireless communications are often described as the next telecom frontier. As such, in-building environments have received much attention for this purpose [1]–[4], but other peculiar environments present significant opportunities for the wireless industry. While the characterization of propagation, within tunnel roads and subways, has been the purpose of many investigations in the last 30 years [5]–[10], the study of propagation in an underground environment, such as a mine, was somewhat neglected. In fact, the corresponding open literature has been quite sparse. Some of the accomplished work was limited, with regard to narrowband measurements, to the evaluation of the attenuation of the received field according to the distance in an underground gallery [11], [12]; typically, these measurements were taken at frequencies in the vicinity of 150, 450, and 900 MHz. Other measurements taken around 2 GHz in a wide tunnel (13 m in width), which is not representative of the typical underground mine (generally much narrower with rough surfaces), were the subject of a statistical study, which was limited in its narrowband analysis to examine the amplitude distribution of the envelope of the received signal [13]. To the best of our knowledge, few papers consider propagation measurements in an underground mine [11], [12], [14]–[17], especially when wideband signals are involved.

The results presented in this paper are based on radio-channel measurements made in a real underground mine, i.e., in a former gold mine now operated by the Canadian Center for Minerals and Energy Technology (CANMET) as a mine-technology laboratory in northern Canada. A central frequency of 2.4 GHz has been used throughout the measurements, in order to ensure compatibility with wireless local area network (WLAN) systems, which may be used for various data, voice, and video communication applications.

A standard technique has been used for the narrowband channel measurements. However, due to equipment availability, the wideband channel-measurement system has been based on the frequency channel-sounding technique [18]–[20]. The use of simulations, based on mathematical models, can also be employed [21] to extract important propagation parameters; however, achieving accurate models in a harsh environment, such as an underground mine, is not easy, since the propagation of waves is generally based on multiple reflections, diffraction, and diffusion on the rough sidewalls' surface.

The objective of this paper is to present the main propagation parameters extracted from experimental results, which can be used for communication applications at 2.4 GHz, leading to operational enhancements for the mining industry.

II. Mathematical Model of the Channel

Since the received signal in a multipath channel consists of a series of attenuated, time-delayed, and phase-shifted replicas of the transmitted signal, the discrete mathematical model of the radio channel is given as a complex transfer function in the frequency domain, or as a complex impulse response in the time domain. For a given position of the transmitter (Tx) and the

Manuscript received September 18, 2003; revised July 7, 2004; accepted September 23, 2004. The editor coordinating the review of this paper and approving it for publication is V. K. Bhargava. This work was supported by Bell Nordic Group, Inc. This paper was presented in part at IEEE Globecom 2002 and at IEEE Personal, Indoor and Mobile Radio Communications (PIMRC) 2003.

C. Nerguizian is with Institut National de la Recherche Scientifique-Énergie, Matériaux et Télécommunications (INRS-EMT), Montreal, QC H5A 1K6, Canada, and also with the École Polytechnique de Montréal, Montreal, QC H3T 1J4, Canada (e-mail: chahe.nerguizian@polymtl.ca).

C. L. Despins is with INRS-EMT, Montreal, QC H5A 1K6, Canada, and also with PROMPT-Quebec, Montreal, QC H3A 2R7, Canada (e-mail: cdespins@promptquebec.com).

S. Affès is with INRS-EMT, Montreal, QC H5A 1K6, Canada (e-mail: affes@inrs-emt.uquebec.ca).

M. Djadel is with Bell Nordiq Group, Inc., Val d'Or, QC J9P 1P6, Canada (e-mail: mdjadel@telebec.com).

Digital Object Identifier 10.1109/TWC.2005.853899

receiver (Rx), the complex transfer function and the baseband impulse response can be written, respectively, as

$$H(t,f) = \sum_{i=1}^{N(t)} a_i(t) \mathrm{e}^{j\theta_i(t)} \mathrm{e}^{-j2\pi f \tau_i(t)} \tag{1}$$

$$h(t,\tau) = \sum_{i=1}^{N(t)} a_i(t) \mathrm{e}^{j\theta_i(t)} \delta\left(\tau - \tau_i(t)\right) \tag{2}$$

where $\{a_i(t)\}$, $\{\tau_i(t)\}$, and $\{\theta_i(t)\}$ are random variables expressing the amplitude, excess delay (arrival time), and phase sequences of different multipaths, respectively, while $N(t)$ is the number of multipath components at measurement instant t. $\delta(\cdot)$ represents the Dirac delta function, while i is the multipath component index.

The channel can be assumed to be time invariant if measurements are taken without human activity and with stationary Tx and Rx, and by averaging the results of several sweeps at each location to avoid any effects of temporal variations of the measurements. The complex transfer function and the baseband impulse response may then be simplified, respectively, as

$$H(f) = \sum_{i=1}^{N} a_i \mathrm{e}^{j\theta_i} \mathrm{e}^{-j2\pi f \tau_i} \tag{3}$$

$$h(\tau) = \sum_{i=1}^{N} a_i \mathrm{e}^{j\theta_i} \delta(\tau - \tau_i). \tag{4}$$

It has to be noted that the magnitude of the complex baseband impulse response in decibels is the same as the power-delay profile (PDP) in decibels, i.e., $20\log(|h(\tau)|) = 10\log(\mathrm{PDP})$.

According to the multipath channel model given above, the received signal will be the convolution of the transmitted signal with the complex impulse response plus the channel noise, which is generally modeled by a complex-valued Gaussian process.

Once the complex impulse-response function is determined, important channel-propagation parameters can be extracted, such as the mean excess delay τ_{m}, the rms delay spread τ_{rms}, and the maximum excess delay $\tau_{\max}$ [18], [19]. The rms delay spread gives an estimation of the amount of intersymbol interference (ISI) to be encountered in the channel due to the time dispersion of the transmitted signal. Since, in some environments, τ_{rms} can give an incorrect evaluation of the severity of the multipath, it is useful to also define the maximum excess delay $\tau_{\max}$, which is the delay span between the first crossing above the predefined threshold level and the last crossing below it. The predefined signal-threshold level is important during the extraction of the propagation parameters, since it defines the removal of the noise and calibration errors at positions where the signal is not present (differentiation between received multipath components and thermal noise). Another important parameter, the coherence bandwidth B_{c} may be extracted from the complex transfer function of the channel. It represents the statistical average bandwidth of the channel over which signal-propagation characteristics are correlated. There exists an inverse relationship between B_{c} and τ_{rms} [22].

The path loss for any measurement location can be deduced from narrowband or wideband measurements. From wideband measurements, considering multipath components above the predefined signal-threshold level, the relative multipath total power in the time domain is computed from

$$P = \sum_{i=1}^{N} a_i^2. \tag{5}$$

From narrowband measurements, for a fixed Tx power, the total received power P_{r} decreases with distance d and the linear relationship between power in decibels and $10\log_{10}$ of the distance is given by [20]

$$10\log_{10}\left[P_{\mathrm{r}}(d)\right] = 10\log_{10}[A] - 10n\log_{10}[d] \tag{6}$$

where n is the path-loss exponent, d is the distance of separation between the Tx and the Rx, and A is a constant set by the transmitted power and the measurement-system gain during calibration. When the transmitted power and the measurement-system gain are known, the value of the total received power can be computed from the equation above, which is the vector summation of the complex multipath components.

III. Measurement System

A. Description of the Environment

Measurements were conducted in an underground gallery of a former gold mine, the laboratory mine "CANMET" in Val d'Or, 700 km north of Montreal, QC, Canada. Located at a 40-m underground level, the gallery stretches over a length of 75 m with a width and height both of approximately 5 m. Fig. 1 illustrates the map of the gallery with all its adjacent galleries. The presence of a closed heated room (for equipment-storage purposes) is noticeable at the beginning of the gallery. Due to the curvature at the end of the gallery, non-line-of-sight (NLOS) propagation is obtained for the last 10 m. The digital photograph, given in Fig. 2, shows a part of the underground gallery. It can be seen from the photograph that the walls are very rough and are protected with a metallic grid, the floor is not flat, and it contains some water plaques.

B. Measurement Setup

A radio-frequency (RF) synthesizer (Tx) and a spectrum analyzer (Rx) have been used for narrowband measurements. For wideband measurements, a vector network analyzer has performed the transmission and the reception of the RF signal.

1) Narrowband Measurement Setup: For the narrowband measurements, an HP83650A synthesizer has been used as the source for the Tx. Its frequency range was between 10 MHz and 50 GHz and the maximum power at the operating frequency of 2.4 GHz was 12 dBm. Omnidirectional S2400B antennas from Cushcraft were used for both transmission and reception. The central frequency of the antennas was 2.4 GHz with a gain of 0 dBi. An HP8563E spectrum analyzer was used as

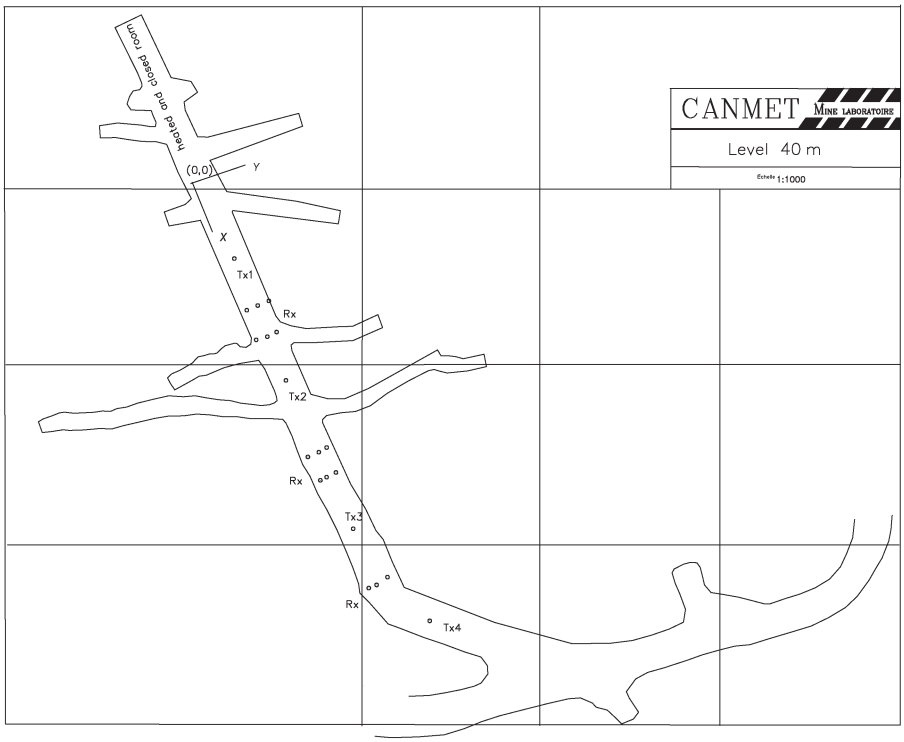

Fig. 1. Map of the underground gallery with the narrowband measurement setup.

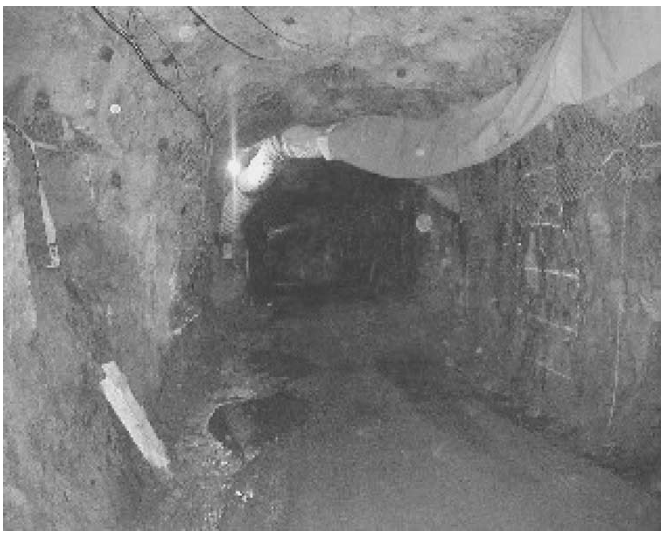

Fig. 2. Digital photograph of the underground gallery.

the Rx. The zero-span mode of the analyzer acted as an envelope detector. The bandwidth of the analyzer's filters (bandpass and low pass) was set to 100 Hz. A set of 601 measurement points, for each location, have been registered by the analyzer, corresponding to a sweep time of 1.2 s and a sampling frequency of 500 Hz (number of points divided by the sweep time), respecting the Nyquist criteria. A National Instrument acquisition card installed in a portable computer with the Labview software was used for data acquisition. It has to be noted that no synchronization cable, between the Tx and the Rx, was needed since the 2.4-GHz frequency of operation was in the operating range of the spectrum analyzer. The analyzer's maximum operating frequency being 26 GHz, no mixing operation was involved. Hence, the problem of synchronization between local oscillators of the Tx and the Rx was avoided.

2) Wideband Measurement Setup: The impulse response of the multipath radio channel can be found by using time-domain techniques, such as measurements using spread-spectrum signals [23] or measurements using the direct pulse-transmission method [24]. In the spread-spectrum method, a maximal-length pseudonoise (PN) code modulates the carrier and is sent into the channel. At the Rx, the PN code is demodulated and correlated with an identical code with a slightly lower rate. The correlation function traced by the Rx gives an estimate of the impulse response of the channel [20]. Using frequency-domain measurements, the complex impulse response of the channel is deduced from its transfer function by taking the inverse Fourier transform (IFT). A band of swept frequencies is sent into the channel. Then, the received frequency components are compared to the transmitted frequencies through a vector network analyzer and the complex transfer function of the channel is found. Due to equipment availability, the coherent frequency response measurements have been used (this method works well for indoor applications, since the distances involved are short). Fig. 3 gives the schematic diagram of the setup for wideband measurements. The main component of the measurement system is the HP8753E vector network analyzer from Hewlett-Packard, which measures the frequency response of the indoor channel. A Matlab file has been used for data postprocessing, to compute the channel impulse response from the measured frequency response of the channel.

During the measurement campaign, the selected frequency band was centered at 2.4 GHz with a span (measurement bandwidth) of 200 MHz, corresponding to a time resolution of about 5 ns. In practice, due to the use of windowing, which

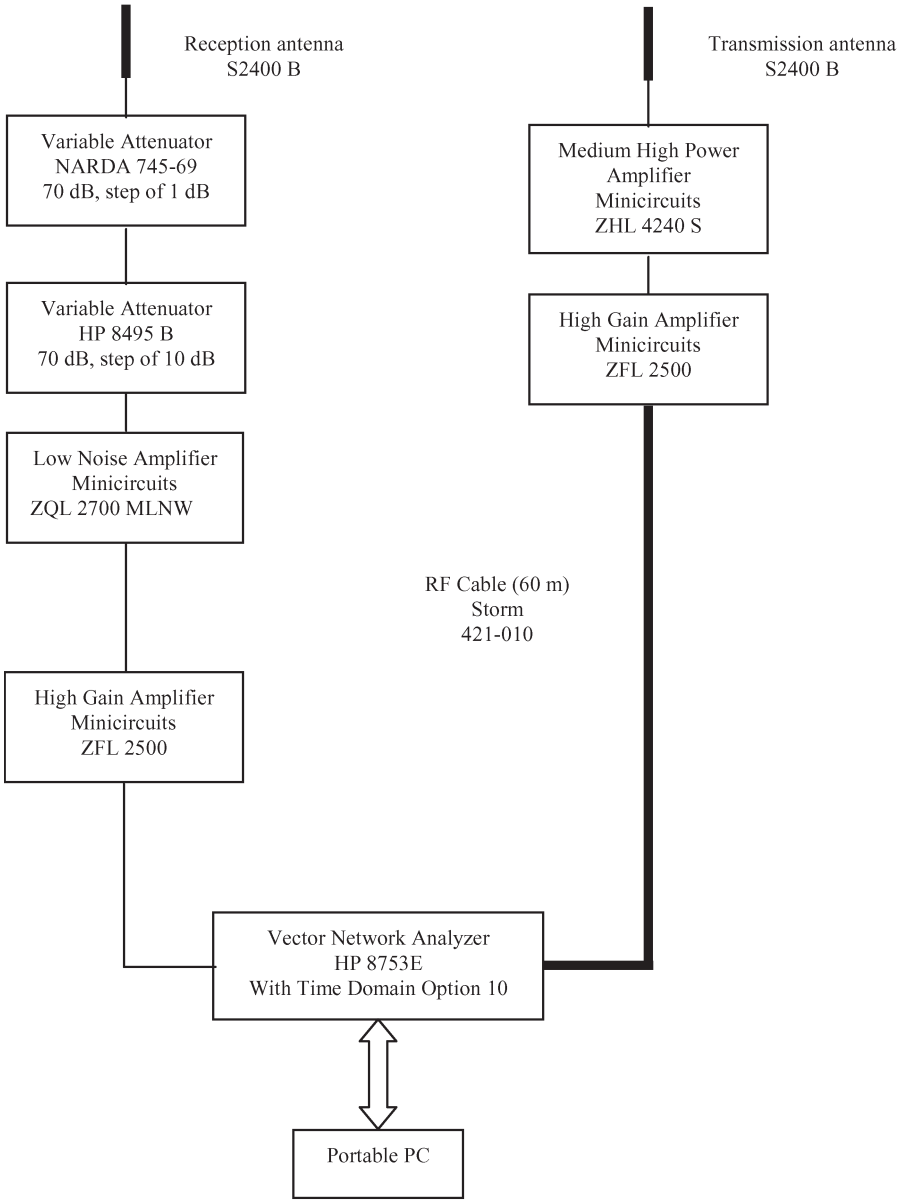

Fig. 3. Schematic diagram of the wideband measurement system.

has the role of suppressing the undesired sidelobes during the IFT operation, this number is multiplied by a constant whose value depends on the type of the chosen window function. By choosing a Hanning window function, which is a good compromise between the main peak width and sidelobe suppression, a peak width widening of 1.5 may occur that multiplies the time-resolution value by 1.5 (for a window with sidelobe level equal to -44 dB, the time resolution will be multiplied by 2). To improve the time resolution of the impulse response or to be able to distinguish more indoor multipath components arriving close to each other, one has to increase the span of the frequency band. However, due to the limited bandwidth of the transmission and reception antennas (about 200 MHz), the measurement bandwidth was set to 200 MHz.

On the other hand, the sweep time of the network analyzer has been decreased to validate the quasi-static assumption of the channel. To do so, each sweep consisted of 201 points or complex samples spaced 1 MHz from each other (200 MHz divided by 201 points). The corresponding unambiguous delay time (range resolution) of 1 μs (inverse of the frequency-sample spacing [25]) was far beyond the sum of the maximum excess delay $\tau_{\max}$ encountered in indoor environments [1], [20] and the propagation delay of the cable. Hence, the occurrence of aliasing was minimized.

Different types of amplifiers were used in the wideband measurement system (Fig. 3). The main characteristics of these amplifiers were the band of operation frequencies, the gain, the maximum output power, and the maximum input power, which is an important variable to avoid any damage to these components. Since the mobile Tx had to move all over the underground gallery, a 60-m RF cable was connected between the source portion of the network analyzer and the high-gain amplifier. At the frequency of 2.4 GHz, the cable (whose operation frequency is between 2 and 18 GHz) showed an attenuation of 26 dB and a delay of 270 ns. The output power of the HP8753E's built-in synthesizer source was set to -10 dBm,

to avoid any damage to the amplifiers. A power level of about 30 dBm has been used at transmission in order to detect weak signals at the Rx, since the channel exhibits an approximate attenuation of 100 dB due to signal propagation when a maximum separation distance between the Tx and the Rx is considered [9], [10]. A 3-m RF cable has been employed to connect the output of the power amplifier to the Tx antenna. At 2.4 GHz, the attenuation of this cable was about 1.9 dB.

The receiving portion of the measurement system consisted of the receiving antenna, two passive cascaded step attenuators of 70 dB each, a low-noise amplifier, a high-gain amplifier, and the Rx portion of the network analyzer. An RF cable of 3 m has been used between the antenna and the first step attenuator. The attenuators were necessary to avoid any damage to the amplifiers since, when the two antennas are close to each other (for a short distance of separation), the level of the received signal can be as high as the transmitted power.

In the case where the signal level at the Rx is maximum (when the two antennas are removed, and transmission and reception chains are connected with each other), the value of the attenuators must be high to limit the input power at the low-noise amplifier. This case corresponds to the calibration of the measurement system, which is necessary in order to remove the effects of the measuring equipment. It has to be noted that the effect of the two antennas is not included in this kind of calibration. However, since the antennas have a low voltage standing wave ratio (VSWR), one can assume that the calibration process described above will remove the effects of the measurement equipment, including the two antennas [26].

In the case where the signal level at the Rx is minimal (when the antennas are separated from each other by the total length of the underground gallery), the value of the attenuators must be set to zero, in order to have an acceptable reception of the weak signal.

In the cases where the separation distance of the antennas is varied, the step attenuators must be varied consequently to have, at the same time, an acceptable reception of the signal and an acceptable input power of the low-noise amplifier to avoid any damage. During the calibration process (connection of the transmission and reception chains in order to embed the effects of the measuring equipment and components, as well as the *RF* cables, into the network analyzer) defined as in [26], the signal level at the input of the first attenuator was around 26 dBm. The attenuator level was selected as 84 dB to avoid damage to the amplifiers.

C. Measurement Procedure

Two different experimental procedures (for narrowband and wideband measurements) have been defined to assess various characteristics of the channel, in order to achieve a successful communication link in the underground gallery. The objective of the narrowband measurements was to assess the power–distance relationship of the channel and notably the impact of the relative position of the transceiver unit and the mine-shaft wall (thus affecting the antenna pattern) on the received power. The wideband measurements were then performed in order to characterize a broad set of wideband parameters of the channel by using an experimental procedure that is more realistic from an underground-mine-operation perspective.

1) Narrowband Measurement Procedure: Four sets of measurements were taken, with the Tx (i.e., the synthesizer and the transmit antenna) placed at a different location for each set. The Rx, consisting of the spectrum analyzer, the personal computer (PC), and the receive antenna, was moved (at both sides of the fixed antenna, i.e., the Tx) to a new position for each power measurement. The position of the Tx for the four sets was ($x = 8$ m, $y = 1.5$ m) for Tx1, ($x = 25$ m, $y = 0.5$ m) for Tx2, ($x = 39$ m, $y = 0.5$ m) for Tx3, and ($x = 56$ m, $y = 0.5$ m) for Tx4, with respect to the predefined referential (Fig. 1). The predefined referential has $x = 0$ at the end of the mine shaft (at the entrance of the closed heated room), while the $y = 0$ position corresponds to the closest position to the wall. Noticeably, Tx2, Tx3, and Tx4 are closer to the wall than Tx1. As for the mobile Rx (circular dots in Fig. 1), it covered the entire underground gallery (situations with LOS and with few NLOS) by varying its position 1 m widthwise (3 positions distant of 1 m for the gallery width of 5 m) and 2 m lengthwise (35 positions distant of 2 m for the gallery length of 70 m). Some other extra intermediate positions have also been used for the NLOS cases, giving a total of 115 measurement points for each Tx location.

2) Wideband Measurement Procedure: The network analyzer and the PC were stationed with the receive antenna and the other Rx components at the predefined referential (Fig. 4, i.e., on the mine-shaft wall). The equipment were calibrated in the presence of the RF cables, as described in the previous section. The transmit antenna and the other Tx components were moved to different locations (circular dots in Fig. 4) within the underground gallery by varying their position 0.5 m widthwise (6 positions separated by 0.5 m for the gallery width of 5 m) and 1 m lengthwise (70 positions separated by 1 m for the gallery length of 70 m). Some other extra intermediate positions have also been used for the LOS and NLOS cases, giving a total of 490 measurement locations among which only 20 measurement locations corresponded to NLOS cases.

It should be noted that these measurements were not made in both directions along the gallery from the fixed transceiver unit (i.e., the Rx, in this case) as they were in the narrowband case. Moreover, the Rx was fixed very close to the mine shaft, whereas it was situated further from the wall (0.5 or 1.5 m) for the narrowband measurements. In addition, due to the availability of the limited-length RF cable and due to the right-angle corner following the curvature at the end of the gallery (beyond which the signal is below the noise floor), only 70 m of the gallery length have been considered. During the measurement campaign, the transmit and receive antennas were both mounted on carts at a height of 1.9 m, replicating the receive antenna placed on the wall and the transmit antenna placed on the helmet of a miner.

IV. Experimental Results

From the narrowband measurements, the path-loss exponent n of the channel has been determined. From the wideband

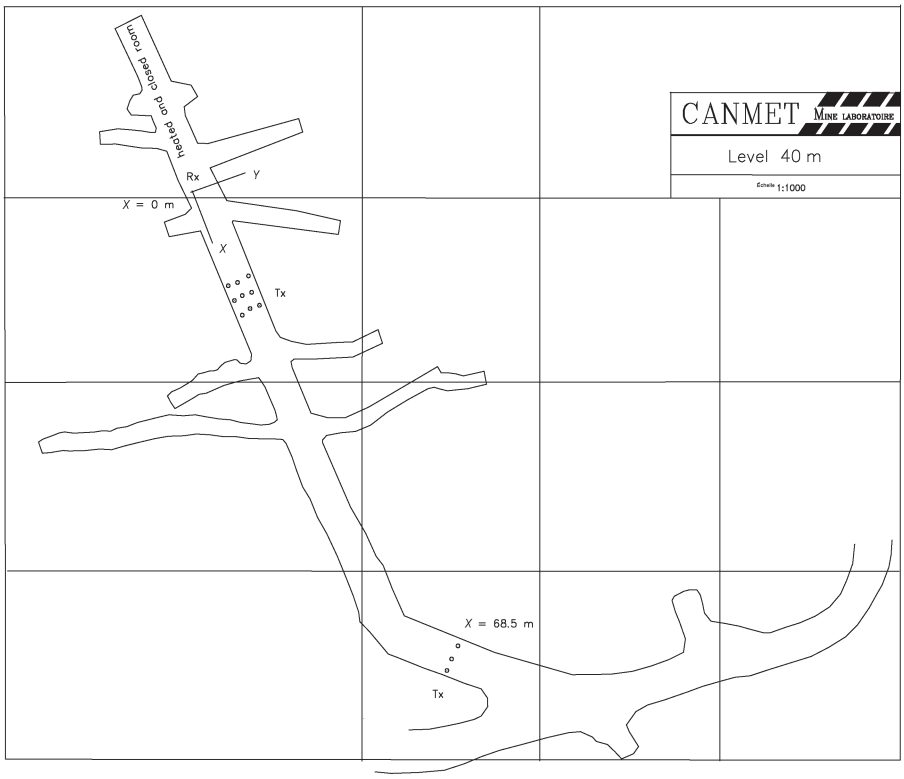

Fig. 4. Map of the underground gallery with the wideband measurement setup.

measurements, the magnitude of the impulse response has been determined and several relevant parameters, such as the mean excess delay τ_{m}, the rms delay spread τ_{rms}, the maximum excess delay $\tau_{\max}$, the coherence bandwidth B_{c}, the relative multipath total power P, the number of multipath components N, and the power and the arrival time of the first multipath component P_1 and τ_1 of the channel have been extracted.

A. Narrowband Experimental Results and Analysis

1) Power–Distance Relationship of the Channel: The total received power P_{r}, measured at all 115 measurement locations with four different Tx locations, as a function of the distance d (consisting of measurement locations situated at both sides of the Txs) is shown in Fig. 5. Using the linear regression fit to process the four sets of measurement data, path-loss exponent values of the channel have been found to be equal to 2.13, 2.33, 2.15, and 2.17, respectively. It is important to note that the path-loss exponent value (for each of the four sets of measurements) is a global one computed over the entire length of the gallery for both LOS and NLOS situations, as well as with the impact of adjacent galleries. Variations of path loss in specific regions of the gallery are emphasized in the section describing the wideband-measurement results.

On the other hand, the results showed a greater variability (standard deviation) of the received power when the Tx is closer to the mine-shaft wall.

Finally, the value of the path-loss exponent, for the combined four sets of data, has been determined to be equal to 2.16 with a standard deviation (σ) of 6.13 between the received-power data and the linear-regression line.

2) Power–Distance Relationship of the Channel Along a Predefined Walk: The total received power P_{r} can provide a simple means for inferring user location. To visualize the correlation between the received power and the spatial location of a user, a plot of the total received power from each Tx (Tx1, Tx2, Tx3, and Tx4) as a function of the distance along a walk (the walk or the movement of the Rx starting from the predefined reference and terminating at the end of the gallery) is given in Fig. 6. Not surprisingly, the signal power at the user or the Rx is the strongest when the Tx is close to it and weakest when it is far away. Moreover, results of the received power, for the four different Tx positions (sets of measurements taken at both sides of the Tx), show site-specific characteristics, notably as a result of the adjacent galleries and the NLOS cases seen by the Tx located at different positions (Tx1, Tx2, Tx3, and Tx4) in the underground gallery.

B. Wideband Experimental Results and Analysis

1) Typical Frequency Response Function of the Channel $H(f)$: The complex transfer function was obtained at all 490 measurement locations. For each location, a temporal average has been performed on a set of ten measurements of different observation times. Notches found in the magnitude (decibel) of a typical frequency response (Fig. 7), as measured by the network analyzer, illustrate the frequency-selective nature of fading in the indoor-gallery channel.

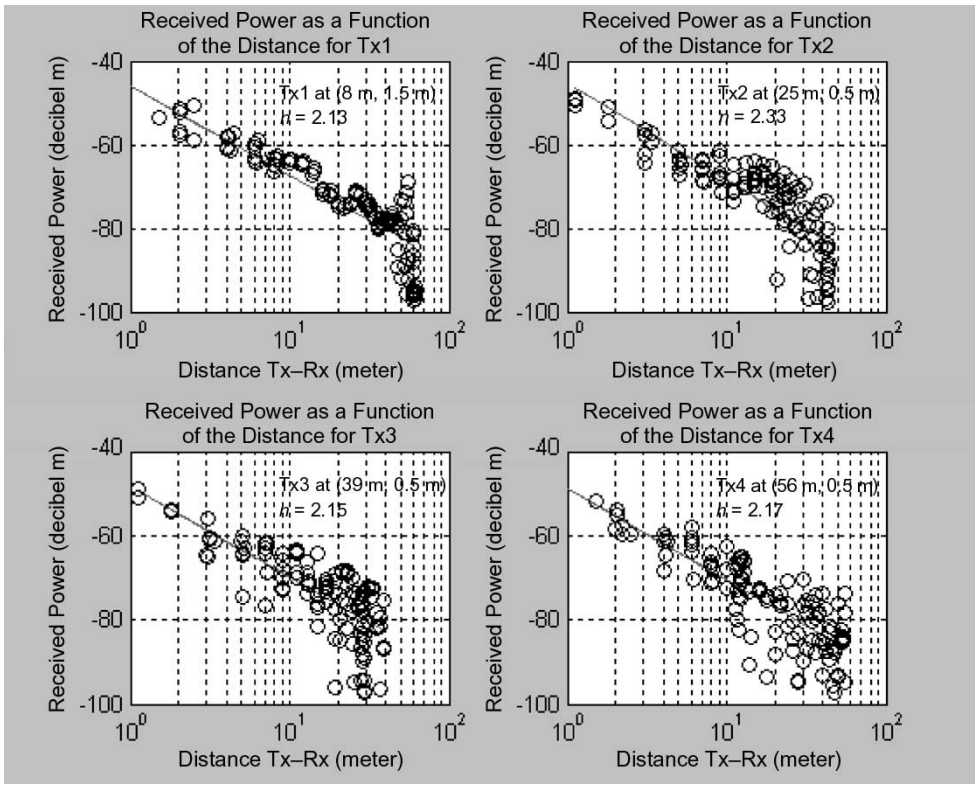

Fig. 5. Total received power as a function of Tx–Rx distance with four different transmitter locations.

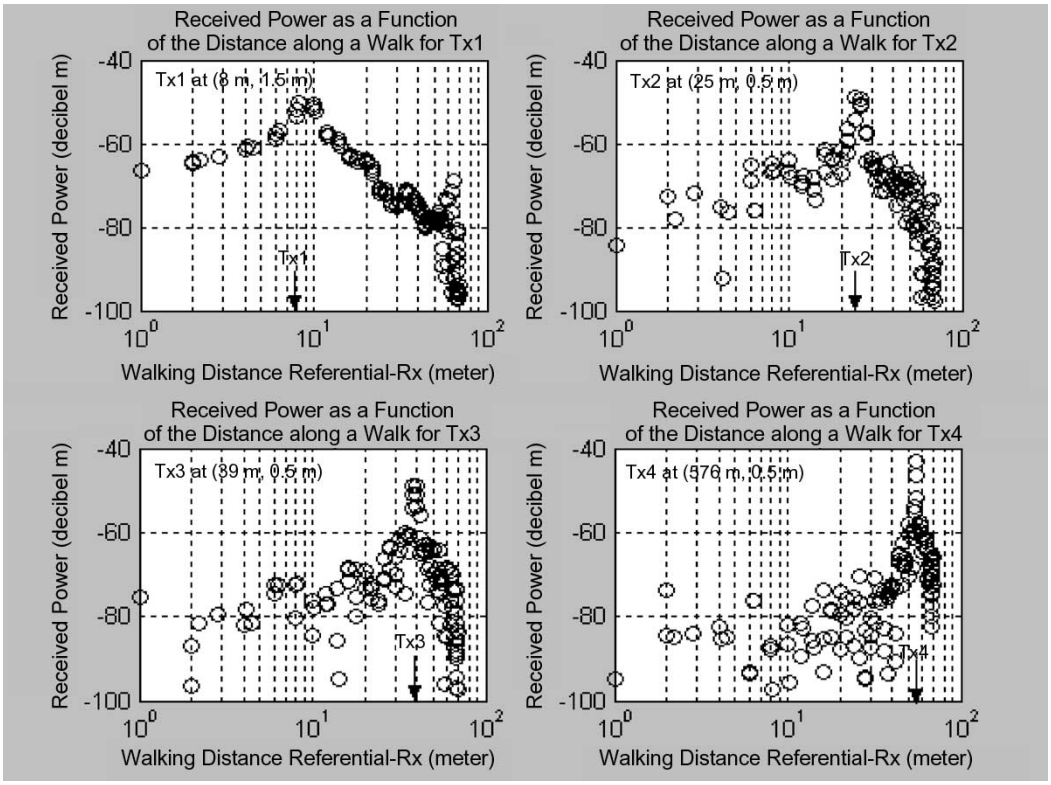

Fig. 6. Total received power from four transmitters as a function of distance along a walk in the underground gallery (distance between Rx and the predefined referential).

2) Typical Magnitude of the Complex Impulse Response of the Channel $|h(\tau)|$: The time-domain magnitude of the complex impulse response $|h(\tau)|$ has been obtained (with a time sampling of 2 ns) from the measured samples of the frequency-domain response using the IFT. Magnitudes of the computed complex impulse response, for typical LOS and NLOS cases,

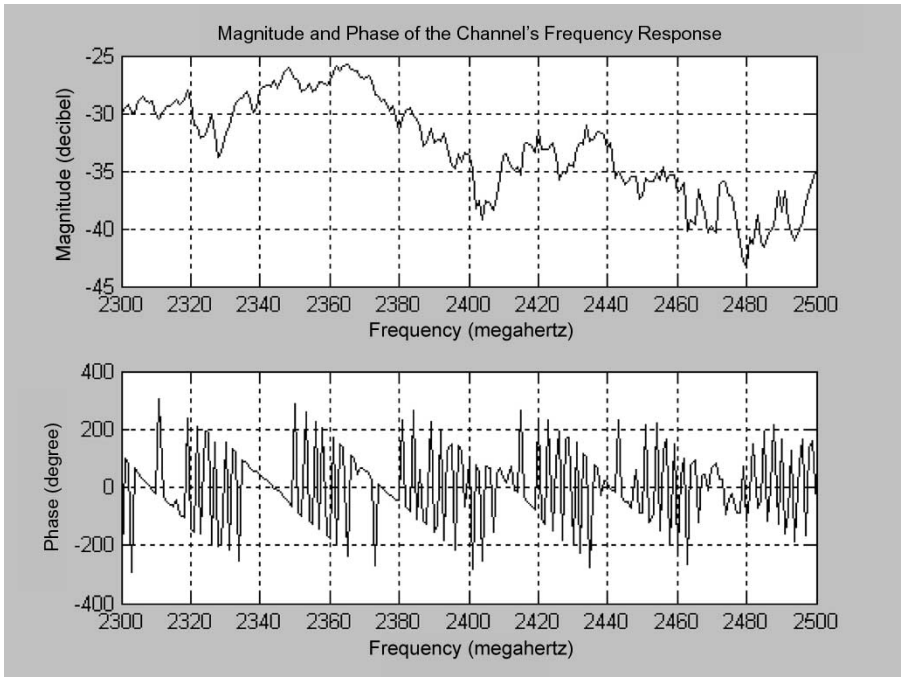

Fig. 7. Magnitude (decibel) and phase (degree) of a typical measured frequency response.

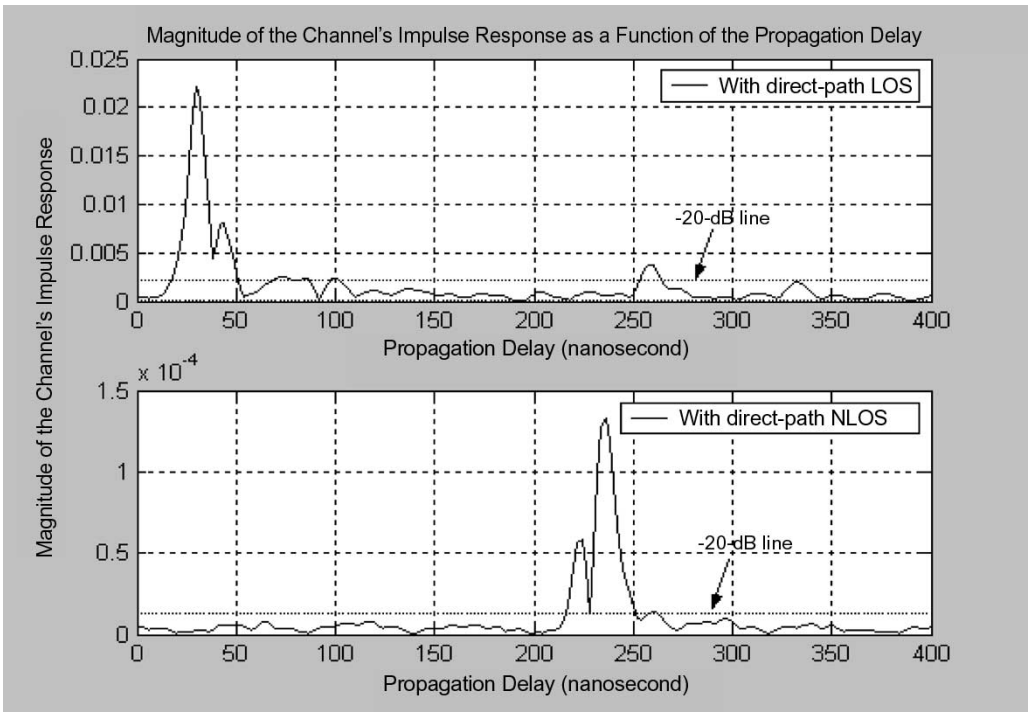

Fig. 8. Magnitudes of the complex impulse response corresponding to the LOS and NLOS cases.

show a first arriving component and many multipath components with various propagation delays (Fig. 8).

3) Parameters Characterizing the Temporal Spread of the Channel: The mean excess delay τ_{m}, the rms delay spread τ_{rms}, and the maximum excess delay $\tau_{\max}$ have been computed for all 490 measurement locations by using predefined thresholds for the multipath noise floor. The four chosen thresholds, referenced to the maximum value of $|h(\tau)|$, were 10, 15, 20, and 26 dB. Two sets of parameters, using a threshold value of 20 dB and a threshold equal to the average of the noise plus four times its standard deviation, have been computed. A comparison between the two results showed negligible differences. Hence, the threshold value of 20 dB, considered as a relevant choice for reliable channel-parameter estimation, has been chosen in order to avoid the effect of noise on the statistics of multipath arrival times.

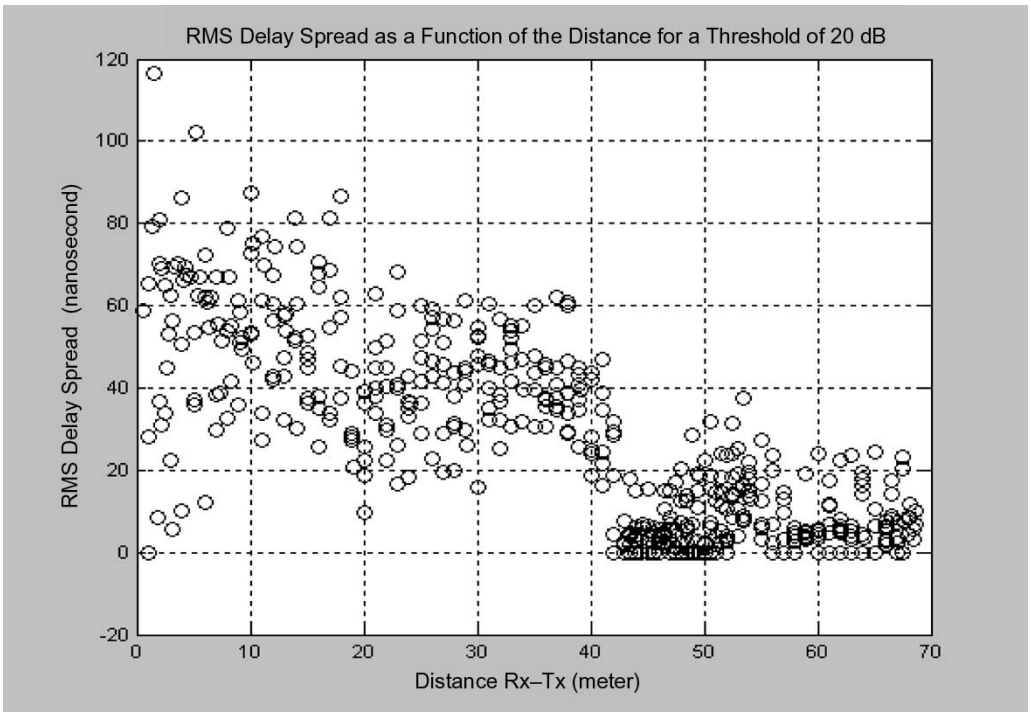

Fig. 9. RMS delay spread as a function of the distance, for a threshold value of 20 dB.

The plot of τ_{rms}, for a threshold of 20 dB, as a function of distance, is shown in Fig. 9. For in-building environments, in which the Tx and the Rx are confined to a closed structure, the reported τ_{rms}-distance profile in [18], [19], and [27] follows a dual-slope relation in which τ_{rms} increases with distance and decreases again after a certain separation between Tx and Rx. For the considered underground gallery, the profile seen in Fig. 9 does not follow a relationship similar to those observed in [18], [19], and [27]. Results show a propagation behavior that is specific for these underground environments. This is likely due to scattering on the rough sidewalls' surface that exhibits a difference of 25 cm between the maximum and minimum surface variations. Moreover, the dependence of τ_{rms} on the bidimensional position of the user is found to be very significant. On the other hand, the τ_{rms}-distance profile shows a multimode behavior depending on the different sections of the underground gallery (areas of propagation dictated by measurement points close to the adjacent galleries and the curvature of the gallery). For a Tx located beyond the point of curvature of the underground gallery, τ_{rms} has a relatively small value compared to the cases where the Tx is closer to the Rx. This is probably due to the high path loss of the channel (Tx located at the far region of the Rx with NLOS conditions), which eliminates the multipath components arriving with longer delays and reduces the number of detectable paths, implying a decrease of the τ_{rms} value. As for the mean excess delay, the computed values did not show a tangible relationship between τ_{m} and the Tx–Rx separation distance.

In order to identify the effect of the predefined threshold on τ_{rms}, its cumulative distribution function has been computed and its curve has been plotted in Fig. 10 for the four chosen threshold values (10, 15, 20, and 26 dB). It can be seen from Fig. 10 that for 50% of all locations, in the investigated underground gallery, τ_{rms} is equal to or less than 6, 12, 24, and 32 ns for threshold values of 10, 15, 20, and 26 dB. For the same four threshold values, τ_{m} is equal to 11, 15, 22, and 75 ns and the value of $\tau_{\max}$ is given by 33, 108, 188, and 338 ns, respectively. The mean, standard deviation, and maximum values of τ_{m}, τ_{rms}, and $\tau_{\max}$ for the four different threshold values are summarized in Table I.

On the other hand, it is possible to characterize the rms delay spread of the channel in the frequency domain by using its coherence bandwidth B_{c}. The value of B_{c} (for a correlation coefficient of 0.5) has been computed for all 490 measurement locations and, as expected, its profile showed an inverse behavior with respect to the profile of τ_{rms}. By using a linear regression between B_{c} and τ_{rms}, the following equation of a straight line has been obtained

$$B_{\mathrm{c}}(\mathrm{MHz}) = -0.56\tau_{\mathrm{rms}}(ns) + 40.4. \tag{7}$$

Finally, the relative multipath total power P has been computed (5) for all 490 measurement locations, and the number of multipath components N has been extracted from the impulse response of the channel.

Fig. 11 gives the variations of P as a function of the Tx–Rx separation distance for a threshold of 20 dB. The plot of Fig. 11 shows distinct areas of propagation separated by the zone of adjacent galleries and by the point of curvature of the underground gallery, as reported in [17]. For the region starting from the predefined referential until the zone of adjacent galleries (mostly LOS propagation), the decrease of the relative multipath total power with distance is less severe than the other sections of the gallery. When the Tx is located

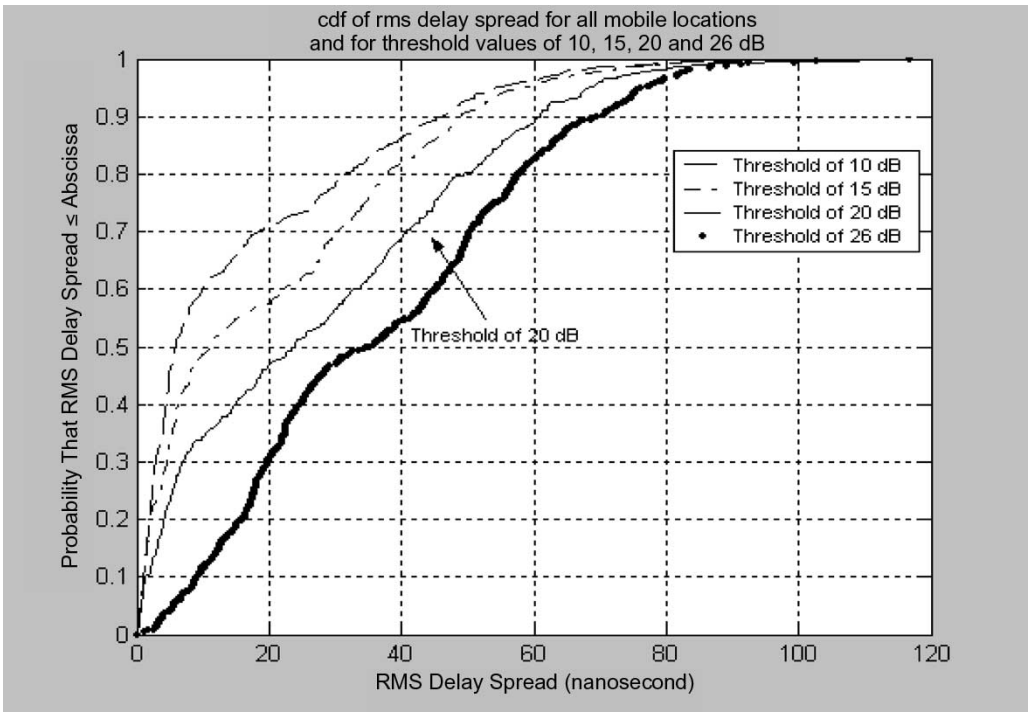

Fig. 10. Cumulative distribution function of τ_{rms} for the four different threshold values.

TABLE I
MEAN, STANDARD DEVIATION, AND MAXIMUM VALUES OF τ_{m}, τ_{rms} AND τ_{max} FOR THE FOUR DIFFERENT THRESHOLD VALUES

	τ_{m} (nanosecond)			τ_{rms} (nanosecond)			τ_{max} (nanosecond)		
Threshold (decibel)	Mean	Standard Deviation	Maximum	Mean	Standard Deviation	Maximum	Mean	Standard Deviation	Maximum
10	8.7	10.6	69.4	15.2	19.1	99.4	62	86.9	384
15	11.2	12.2	77	19.8	20.3	99	89.4	95.9	384
20	16.5	20	127.2	27.4	23.3	116.4	152.2	119.4	388
26	57.2	53.2	229.2	37.1	23	116.8	271.9	99.1	394

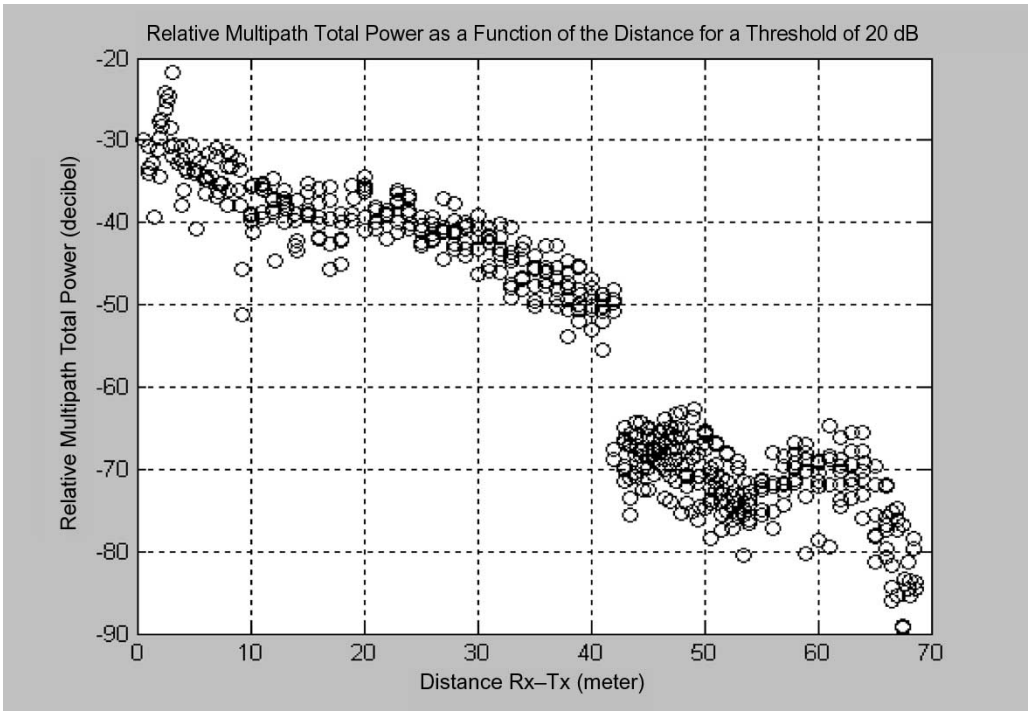

Fig. 11. Relative multipath total power as a function of the distance, for a threshold value of 20 dB.

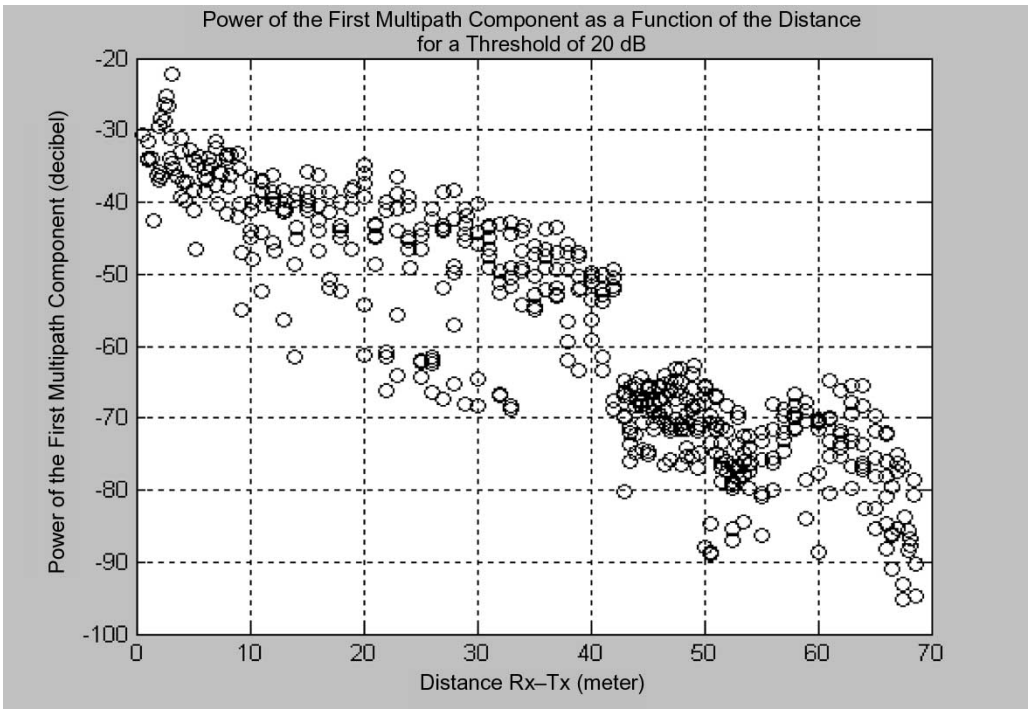

Fig. 12. Power of the first multipath component as a function of the distance, for a threshold value of 20 dB.

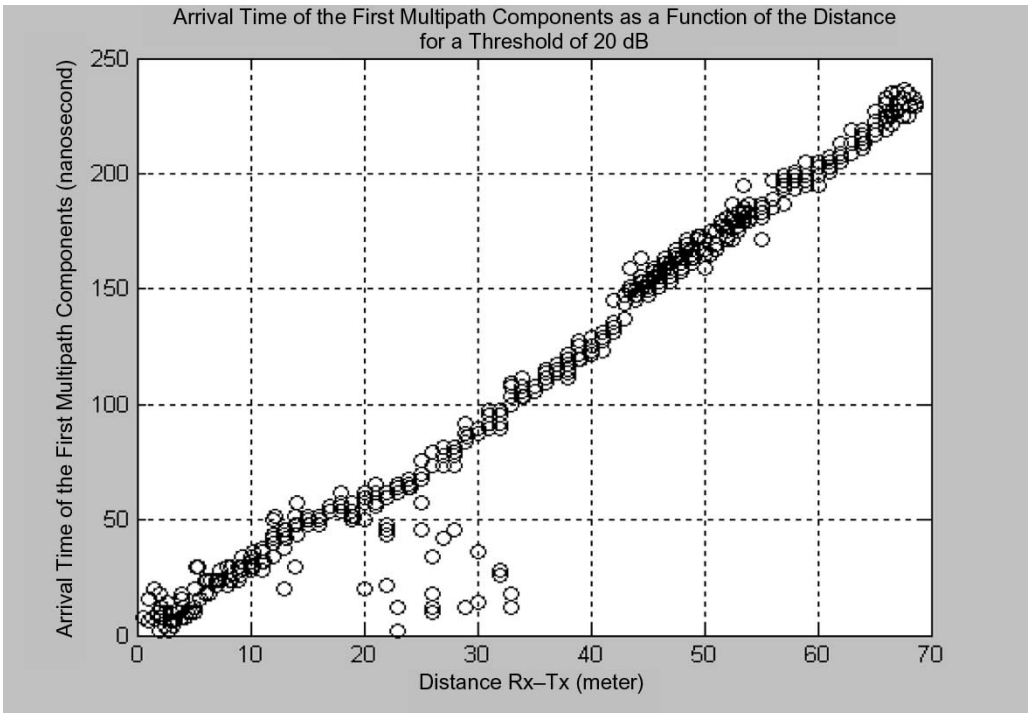

Fig. 13. Arrival time of the first multipath component as a function of the distance, for a threshold value of 20 dB.

between the entrance of the adjacent galleries and the point of curvature, the Rx sees a higher transmit-signal attenuation because of extra propagation path losses in the adjacent galleries. For the region starting from the curvature until the end of the gallery (mostly NLOS propagation), the signal attenuation is the highest.

On the other hand, the τ_{rms}-distance and N-distance profiles (obtained from the computed values) exhibit similar variations confirming that, for the far region, multipath components arriving with longer delays and subjected to a high path loss are not detectable. Moreover, it has been noticed that the application of the threshold value, to screen multipath components, affected the value of N significantly. The mean, the standard deviation, and the maximum values of N for all locations, using a threshold of 20 dB, have been found to be equal to 7, 5, and 25, respectively.

4) Other Parameters Describing the Type of Signal Visibility (LOS, NLOS): Due to the topology of the considered underground gallery, both LOS and NLOS cases may be encountered. When there is direct visibility between the Tx and the Rx, the magnitude of the first path is the highest compared to the other multipath components. For the NLOS situation, the magnitude of the first path is not necessarily the strongest. In order to identify the type of signal visibility (LOS or NLOS), the power and the arrival time of the first path have been determined from the impulse response of the channel by considering all of the 490 measurement locations. Figs. 12 and 13 give the variations of P_1 and τ_1 as a function of the Tx–Rx separation distance for a threshold value of 20 dB.

It can be seen that the P-distance and P_1-distance profiles obtained in Figs. 11 and 12 exhibit similar behaviors. This result was predictable since, for the considered environment, only 5% of the measurement locations correspond to the NLOS situations. Accordingly, for the majority of locations (mostly LOS), P_1 (power of the first path) is dominant and its value is close to P (algebraic-power sum of all multipath components).

As for the arrival time of the first path, the τ_1-distance profile (see Fig. 13) shows a straight-line behavior with a slope equal to the inverse of the signal-propagation speed (3.33 ns/m). Moreover, the computed standard deviation of τ_1, with respect to the approximated straight-line, is equal to 14.5 ns.

V. Conclusion

The results of the wideband measurements show that the τ_{rms}-distance profile is specific to the studied underground gallery and does not follow a dual-slope relation with respect to distance. Due to the rough sidewalls' surface, the dependence of the rms delay spread on the bidimensional position of the user is found to be very significant. Furthermore, for the majority of locations (90% of the cases), values of τ_{rms} (for a threshold of 20 dB) are less than 60 ns. On the other hand, the coherence bandwidth, computed from the mean value of τ_{rms}, is approximately equal to 7 MHz (the inverse of five times the τ_{rms} mean value). Hence, when transmitting a signal having a bandwidth larger than 7 MHz through the considered underground gallery, frequency-selective effects will be observed in the channel. Finally, it has been noted that, for the studied underground gallery with low human activity, the impulse response of the channel is reproducible and respects the uniqueness property (the impulse response of the channel in one location is relatively different from the one in another location).

Acknowledgment

The authors wish to thank M. A. Belyazid for his precious help in the measurement campaign.

References

[1] H. Hashemi, "The indoor radio propagation channel," *Proc. IEEE,* vol. 81, no. 7, pp. 943–968, Jul. 1993.

[2] T. S. Rappaport, "Characterization of UHF multipath radio channels in factory buildings," *IEEE Trans. Antennas Propag.*, vol. 37, no. 8, pp. 1058–1069, Aug. 1989.

[3] D. M. J. Devasirvatham, "A comparison of time delay spread and signal level measurements within two dissimilar office buildings," *IEEE Trans. Antennas Propag.*, vol. 35, no. 3, pp. 319–324, Mar. 1987.

[4] L. Talbi and G. Y. Delisle, "Experimental characterization of EHF multipath indoor radio channels," *IEEE J. Sel. Areas Commun.*, vol. 14, no. 3, pp. 431–440, Apr. 1996.

[5] P. Delogne, "Basic mechanisms of tunnel propagation," *Radio Sci.*, vol. 11, no. 4, pp. 295–303, 1976.

[6] S. F. Mahmoud and J. R. Wait, "Geometrical optical approach for electromagnetic wave propagation in rectangular mine tunnels," *Radio Sci.*, vol. 9, no. 12, pp. 1147–1158, 1974.

[7] P. Mariage, M. Liénard, and P. Degauque, "Theoretical and experimental approach of the propagation of high frequency waves in road tunnels," *IEEE Trans. Antennas Propag.*, vol. 42, no. 1, pp. 75–81, Jan. 1994.

[8] M. Liénard, P. Lefèvre, and P. Degauque, "Remarques concernant le calcul de propagation d'ondes haute fréquence en tunnel," *Ann. Télécommun.*, vol. 52, no. 9–10, p. 529, 1997.

[9] Y. Hwang, Y. P. Zhang, and G. Kouyoumjian, "Ray-optical prediction of radio-wave propagation characteristics in tunnel environments—Part I: Theory," *IEEE Trans. Antennas Propag.*, vol. 46, no. 9, pp. 1328–1336, Sep. 1998.

[10] Y. P. Zhang, Y. Hwang, and G. Kouyoumjian, "Ray-optical prediction of radio-wave propagation characteristics in tunnel environments—Part II: Analysis and measurements," *IEEE Trans. Antennas Propag.*, vol. 46, no. 9, pp. 1337–1345, Sep. 1998.

[11] M. Liénard and P. Degauque, "Natural wave propagation in mine environments," *IEEE Trans. Antennas Propag.*, vol. 48, no. 9, pp. 1326–1339, Sep. 2000.

[12] Y. P. Zhang, G. X. Zheng, and J. H. Sheng, "Radio propagation at 900 MHz in underground coal mines," *IEEE Trans. Antennas Propag.*, vol. 49, no. 5, pp. 757–762, May 2001.

[13] M. Liénard and P. Degauque, "Propagation in wide tunnels at 2 GHz: A statistical analysis," *IEEE Trans. Veh. Technol*, vol. 47, no. 4, pp. 1322–1328, Nov. 1998.

[14] M. Hämäläinen, J. Talvitie, V. Hovinen, and P. Leppänen, "Wideband radio channel measurement in a mine," in *Proc. IEEE 5th Int. Symp. Spread Spectrum Techniques and Applications*, Sun City, South Africa, Sep. 1998, vol. 2, pp. 522–526.

[15] M. Liénard and P. Degauque, "Mobile telecommunication in mine: Characterization of radio channel," in *Proc. 8th Mediterranean Electrotechnical Conf. (MELECON)*, Bari, Italy, 1996, vol. 3, pp. 1663–1665.

[16] B. L. F. Daku, W. Hawkins, and A. F. Prugger, "Channel measurements in mine tunnels," in *Proc. IEEE 55th Vehicular Technology Conf.*, Birmingham, AL, May 2002, vol. 1, pp. 380–383.

[17] M. Djadel, C. Despins, and S. Affès, "Narrowband propagation characteristics at 2.45 and 18 GHz in underground mining environments," in *Proc. IEEE Global Telecommunications (GLOBECOM)*, Taipei, Taiwan, R.O.C., Nov. 2002, pp. 1870–1874.

[18] A. F. AbouRaddy, S. M. Elnoubi, and A. El-Shafei, "Wideband measurements and modeling of the indoor radio channel at 10 GHz—Part I," in *Proc. 15th Nat. Radio Science Conf.*, Cairo, Egypt, Feb. 1998, pp. B13/1–B13/8.

[19] ——, "Wideband measurements and modeling of the indoor radio channel at 10 GHz—Part II," in *Proc. 15th Nat. Radio Science Conf.*, Cairo, Egypt, Feb. 1998, pp. B14/1–B14/8.

[20] K. Pahlavan and A. H. Levesque, *Wireless Information Networks*. New York: Wiley, 1995.

[21] M. Ndoh and G. Y. Delisle, "Propagation of millimetric waves in rough sidewalls mining environment," in *Proc. IEEE 53rd Vehicular Technology Conf.*, Rhodes, Greece, May 2001, vol. 1, pp. 439–443.

[22] K. Pahlavan, R. Ganesh, and S. J. Howard, "Wideband frequency and time domain models for the indoor radio channel," in *Proc. IEEE Global Telecommunications (GLOBECOM)*, Phoenix, AZ, Dec. 1991, pp. 1135–1140.

[23] D. C. Cox, "Delay doppler characteristics of multipath propagation at 910 MHz in a suburban mobile radio environment," *IEEE Trans. Antennas Propag.*, vol. 20, no. 5, pp. 625–635, Sep. 1972.

[24] A. A. M. Saleh and R. A. Valenzuela, "A statistical model for indoor multipath propagation," *IEEE J. Sel. Areas Commun.*, vol. 5, no. 2, pp. 128–137, Feb. 1987.

[25] G. J. M. Janssen, P. A. Stigter, and R. Prasad, "Wideband indoor channel measurements and BEP analysis of frequency selective multipath channels at 2.4, 4.75 and 11.5 GHz," *IEEE Trans. Commun.*, vol. 44, no. 10, pp. 1272–1288, Oct. 1996.

[26] G. Morrison, H. Zaghloul, M. Fattouche, M. Smith, and A. McGirr, "Frequency measurements of the indoor channel: System evaluation and post processing using IFDT and arma modeling," in *Proc. IEEE Pacific Rim Conf. Communications, Computers and Signal Processing*, Victoria, BC, Canada, May 1991, pp. 71–74.

[27] R. J. C. Bultitude, P. Melançon, H. Zaghloul, G. Morrison, and M. Prokki, "The dependence of indoor channel multipath characteristics on transmit/receive ranges," *IEEE J. Sel. Areas Commun.*, vol. 11, no. 7, pp. 979–990, Sep. 1993.

Chahé Nerguizian (S'01–M'03) received the B.Eng., M.Eng., and Ph.D. degrees in electrical engineering from the École Polytechnique, McGill University and University of Québec INRS-ÉMT (formerly Telecommunications Center), Montréal, QC, Canada, in 1981, 1983, and 2003, respectively.

He joined in 1986, after two years of industrial experience as a Microwave Engineer with Canadian Marconi Canada (Avionic Division), Montréal, QC, Canada, the Department of Electrical and Computer Engineering, École Polytechnique, Montréal, QC, Canada, as a Full-Time Lecturer and became an Assistant Professor in 1994. Currently, he is an Associate Professor in the Telecommunications Group. His research interests are in wireless radio propagation, indoor–outdoor geolocation, and wireless telecommunications.

Prof. Nerguizian is a Member of the Order of Engineers of Québec (OIQ).

Charles L. Despins (S'93–M'94–SM'02) received the B.Eng. degree in electrical engineering from McGill University, Montréal, QC, Canada, in 1984, and the M.Eng. and Ph.D. degrees from Carleton University, Ottawa, ON, Canada, in 1987 and 1991, respectively.

He was, from 1992 to 1996, a Faculty Member of the Institut National de la Recherche Scientifique (INRS), Université du Québec, Montréal, Canada, following employment in 1984–1985 with CAE Electronics as a Member of the Technical Staff, and in 1991–1992 with the Department of Electrical and Computer Engineering, École Polytechnique de Montréal, Canada, as a Lecturer and a Research Engineer. From 1996 to 1998, he was with Microcell Telecommunications, Inc., a Canadian Global System for Mobile (GSM) operator, and was responsible for industry standard and operator working groups, as well as for technology trials and technical support for GSM joint-venture deployments in China and India. From 1998 to 2003, he was Vice-President and Chief Technology Officer of Bell Nordiq Group, Inc., a wireless and wireline network operator in the northern and rural areas of Canada. Since 2003, he has been President of Partnerships for Research on Microelectronics, Photonics and Telecommunications (PROMPT)-Quebec, a university–industry research-partnership organization. He is also an Adjunct Professor at INRS-EMT, Montreal, QC, Canada, at the Université Laval, Québec, QC, Canada and at the University of Alberta, Edmonton, AB, Canada.

Dr. Despins was awarded the IEEE Vehicular Technology Society Best Paper of the Year Prize in 1993. He is a Member of the Order of Engineers of Québec and is also a Fellow of the Engineering Institute of Canada.

Sofiène Affes received the Diplôme d'Ingénieur in electrical engineering in 1992 and the Ph.D. degree with honors in signal and image processing in 1995 from the École Nationale Supérieure des Télécommunications (ENST), Paris, France.

He has been since with INRS-ÉMT (formerly the Telecommunications Center), University of Quebec, Montreal, QC, Canada, as a Research Associate from 1995 until 1997, then as an Assistant Professor until 2000. Currently, he is an Associate Professor in the Personal-Communications Group. His research interests are in statistical signal and array processing, synchronization, and multiuser detection in wireless communications. Previously, he was involved in the European Strategic Program for Research and Development in Information Technology (ESPRIT) projects 2101 Adverse Environment Recognition of Speech (ARS) on speech recognition in adverse environments at Cambridge University (CUED), U.K., in 1991, and 6166 Enhancement of Hands-Free Telecommunications (FREETEL) on hands-free telephony at ENST (Département TSI), France, from 1993 to 1994. In 1997, he participated in the major program in personal and mobile communications of the Canadian Institute for Telecommunications Research (CITR). From 1998 to 2002, he was leading the radio-design and signal-processing activities of the Bell/Nortel/NSERC Industrial Research Chair in Personal Communications at INRS-ÉMT, Montreal, QC, Canada. He currently holds a Canada Research Chair in High-Speed Wireless Communications.

Professor Affes was the corecipient of the 2002 Prize for Research Excellence of INRS.

Mourad Djadel received the B.Eng. and M.Eng degrees in electrical engineering from ENST-Paris, France and the University of Québec INRS-ÉMT (formerly the Telecommunications Center), Montréal, QC, Canada in 1996 and 2002, respectively.

He is presently employed by Bell Nordiq Group, Inc. (Network Technology Direction and Investments), Val d'Or, QC, Canada, as Wireless Networks Manager.